

Mining the Metal-Rich Stars for Planets

Gregory Laughlin¹

¹*NASA Ames Research Center, Moffett Field, CA 94035*

ABSTRACT

We examine the correlation between stellar metallicity and the presence of short-period planets. It appears that approximately 1 % of dwarf stars in the solar neighborhood harbor short-period planets characterized by near-circular orbits and orbital periods $P < 20$ days. However, among the most metal-rich stars (defined as having $[\text{Fe}/\text{H}] > 0.2$ dex), it appears that the fraction increases to 10%. Using the Hipparcos database and the Hauck & Mermilliod (1998) compilation of Strömgren *uvby* photometry, we identify a sample of 206 metal-rich stars of spectral type K, G and F which have an enhanced probability of harboring short-period planets. Many of these stars would be excellent candidates for addition to radial velocity surveys. We have searched the Hipparcos epoch photometry for transiting planets within our 206 star catalog. We find that the quality of the Hipparcos data is not high enough to permit unambiguous transit detections. It is, however, possible to identify candidate transit periods. We then discuss various ramifications of the stellar metallicity – planet connection. First, we show that there is preliminary evidence for increasing metallicity with increasing stellar mass among known planet-bearing stars. This trend can be explained by a scenario in which planet-bearing stars accrete an average of $30 M_{\oplus}$ of rocky material after the gaseous protoplanetary disk phase has ended. We present dynamical calculations which suggest that a survey of metallicities of spectroscopic binary stars can be used to understand the root cause of the stellar metallicity – planet connection.

Subject headings: stars: planetary systems — stars: metallicity

1. Introduction

The discovery of extrasolar planetary systems (Mayor & Queloz 1995, Marcy & Butler 1998, Marcy et al. 2000) has sparked a great deal of excitement. Nearly fifty planets have now been detected around other stars, and the total census has grown to the point where statistical trends are beginning to emerge.

There appears, for example, to be a dearth of objects in the mass range between 10 and 80 Jupiter masses, indicating that brown dwarfs and planets represent two distinct populations, presumably formed via different physical processes. There also appear to be at least two different classes of extrasolar planets. When the orbital period of a planet is less than approximately 20 days,

the orbit tends to be nearly circular, whereas extrasolar planets with longer periods are generally on much more eccentric orbits. In this paper, we will refer to planets with $P < 20$ days as “short-period”. Tidal circularization is inadequate to explain the circular orbits of short-period planets with semi-major axes greater than ~ 0.1 AU (Rasio & Ford 1996, Hut 1981). It is thus likely that many of these planets migrated gradually inward due to interactions with a gaseous protostellar disk (Lin, Bodenheimer & Richardson 1995), although *in situ* formation is also possible (Bodenheimer, Hubickyj & Lissauer 2000). The large eccentricities of the planets with periods longer than 20 days can arise through dynamical interactions between multiple planets (e.g. Levison, Lissauer & Duncan 1998), perturbations from a bound stellar companion (Holman, Touma & Tremaine 1997), and interactions with binary stars in the birth aggregate (Laughlin & Adams 1998).

Our own Solar System presents two more categories: (1) the terrestrial planets, and (2) the Jovian planets on long-period, nearly circular orbits. As the time baseline of the ongoing radial velocity surveys increases, long-period Jupiter-mass planets in other systems will be detectable (Vogt et al. 2000), whereas space-based transit surveys such as the proposed Kepler mission (Borucki et al. 1997; Koch et al. 1998) will be able to detect extrasolar terrestrial planets.

In this paper, we focus attention on another emerging trend. The stars known to harbor extrasolar planets tend to be considerably more metal-rich than the average population I star in the galactic neighborhood. Indications of this correlation were apparent even with the first detections (Gonzalez 1997, 1998, 1999). 51 Peg, for example, has a metallicity $[\text{Fe}/\text{H}] = 0.21$ dex (Gonzalez 2000), which makes it more metal-rich than 98% of the G dwarfs in the Solar Neighborhood (Rocha-Pinto & Maciel 1996). Other planet bearing stars such as BD-10 3166, 55 Cnc, and 14 Her, all with $[\text{Fe}/\text{H}] \sim 0.5$ dex, are among the most metal-rich stars currently known (Castro et al. 1997, Gonzalez et al. 1999).

Extrasolar planet searches have concentrated effort towards surveys of solar-type main sequence stars of spectral type ranging from roughly K5 through F7 (Marcy et al. 2000). These stars are relatively common, and are also relatively bright. Furthermore, solar analogs tend to be photometrically stable, and present a useful variety of absorption lines for radial velocity determination. The current census of planets is therefore concentrated among stars of approximately solar mass. There is, however, no apparent bias against metal-poor stars in the current surveys. Indeed, at a given mass, metal-poor stars are brighter than metal-rich stars. For instance, doubling the metallicity of a $1 M_{\odot}$ ZAMS star from $[\text{Fe}/\text{H}] = 0.00$ to $[\text{Fe}/\text{H}] = 0.30$ leads to a 320 K decrease in surface temperature and a factor of 1.3 decrease in luminosity (Forestini 1994). The current radial velocity searches are essentially magnitude-limited surveys. Metal-poor stars will thus tend to be overrepresented in the target lists.

Furthermore, Brown et al. (2000) have examined the detailed time-series photometry of 34091 stars in the globular cluster 47 Tucanae. Using the Hubble Space Telescope, they collected 8.3 days of data, and expected to find roughly 30 transiting short-period planets, based on the occurrence rate among stars in the radial velocity surveys. No planets were found. The metallicity of 47 Tucanae

is $[\text{Fe}/\text{H}]=-0.7$, which is considerably lower than the metallicity of any star known to harbor an extrasolar planet.

There are now enough planets for us to begin to quantify the short-period planet – stellar metallicity correlation, and to make reasonable estimates of the overall frequency of occurrence of short-period planets. Rocha-Pinto & Maciel (1996) have used the Third Catalog of Nearby Stars (Gliese & Jahreiss 1991) to identify 345 dwarf stars within 25 pc of probable spectral type G0–G9. Within this volume-limited (and essentially complete) sample, three stars (51 Peg, HD 217107, and 55 Cnc) are known to have short-period planets, implying a frequency of occurrence of roughly 1% among solar type stars. This estimate suffers from small number statistics, but is in rough agreement with the initial estimate of 2% by Butler et al. (1997) based on the number of short-period planets found in the original Lick radial velocity survey.

Butler et al. (2000) report that most single G, K, and late F dwarf stars of magnitude $V < 8$ (~ 2000 stars) are presently being monitored by the radial velocity surveys. The Rocha-Pinto & Maciel (1996) census indicates that there should be approximately 1,100 G dwarfs lying within a radius of 40 pc. A majority of these will be brighter than $V=8$, and hence should already be under surveillance. Short-period planets of mass $M_p > 0.3M_{\text{JUP}}$ are readily detected after a year or so of observation. One can thus conclude that the six short-period planets orbiting G dwarfs within 40 parsecs should constitute a reasonable fraction of those which actually exist. It would thus appear that *at least* 0.5% of solar type dwarfs are accompanied by short-period planets.

Finally, Vogt et al. (2000) report that among 1000 stars with more than two years of accumulated data, nine planets with $P < 20$ days have been discovered. All of these estimates are in reasonable concordance, and together suggest that the rate of occurrence of short-period planets among single main sequence stars in the solar neighborhood is of order 1%.

As mentioned above, the stars which bear planets are (on average) enriched in metals in comparison to the Sun, and this trend appears to be particularly strong for the short-period planets (Gonzalez 1997, Butler et al. 2000). In Table 1, we list the properties of currently known planets which have orbital periods of 20 days or less. The logarithmic average metallicity of the primary stars harboring short-period planets is $[\text{Fe}/\text{H}] = 0.16$ dex (excluding HD 83443 for which no metallicity determination or *uvby* photometry currently exists), whereas the logarithmic average metallicity of G dwarfs in the solar neighborhood is $[\text{Fe}/\text{H}] = -0.2$ dex (Rocha-Pinto & Maciel 1996). Of the six G dwarfs in Table 1 which lie within 40 pc, four have metallicity $[\text{Fe}/\text{H}] > 0.2$ dex. Stars of metallicity $[\text{Fe}/\text{H}] > 0.2$ dex constitute a mere 2.4% of the local G dwarf population, and hence about 35 such metal-rich G dwarfs are expected to lie within 40 parsecs. It therefore appears that approximately 10% of stars with $[\text{Fe}/\text{H}] > 0.2$ dex are accompanied by short-period planets. In other words, the most metal-rich stars have a ten times increased probability of harboring a short-period planet. In this paper, we seek to explore the consequences of this remarkable correlation.

This paper is organized as follows: in §2 we compile a catalog of 206 high-metallicity stars which have an increased likelihood of harboring short-period planets. In §3 we search the Hipparcos

epoch photometry for candidate transit events among the 206 stars in the catalog, and discuss the possibility of detecting transiting planets using this method. In §4 we discuss an emerging trend toward increasing metallicity as a function of stellar mass among the known planet-bearing stars. In §5 investigate the possibility of using metallicity measurements of spectroscopic binary stars to determine whether the short-period planet – stellar metallicity correlation arises from the intrinsic properties of the parent star-forming molecular cloud core or, alternately, through post-formation enrichment. We summarize and discuss our results in §6.

2. A Target List of High-Metallicity Stars

The clear existence of a correlation between high stellar metallicity and the presence of a short-period planet indicates that a selective targeting of high metallicity stars would constitute an effective search method. Indeed, this strategy has already yielded success. The formerly obscure star BD-10 3166 was listed by Castro et al. (1997) as one of the five most metal-rich stars known, with $[\text{Fe}/\text{H}] = 0.5$. As reported in Butler et al. (2000), it was added to the Keck Radial Velocity Survey at the suggestion of Gonzalez, Wallerstein & Saar (1999), and was soon thereafter found to harbor a $M \sin i = 0.48 M_{\text{JUP}}$ planet in a 3.487 day low-eccentricity orbit.

Although most dwarf stars with $V < 8$ are currently being targeted by the various radial velocity searches, the total number of stars being surveyed is much smaller than the total population of dwarf stars now known to exist within the broader ($d < 100$ pc) solar neighborhood. It is therefore of interest to compile a list of metal-rich stars that are dim enough to have likely eluded detailed attention thus far.

Spectroscopic abundance analyses exist for only a relatively small number of stars, but there are over 63,300 stars for which *uvby* photometry has been reported in the literature. Furthermore, every individual *uvby* measurement published prior to the middle of 1996 has been compiled in machine-readable form by Hauck & Mermilliod (1998).

Schuster & Nissen (1989) have published a calibration which uses the standard *uvby* indices, $b - y$, m_1 , and c_1 to estimate the metallicity of a given star:

$$[\text{Fe}/\text{H}] = 1.052 - 73.21 m_1 + 280.9 m_1 (b - y) + 333.95 m_1^2 (b - y) - 595.5 m_1 (b - y)^2 + \\ (5.486 - 41.62 m_1 - 7.963 (b - y)) \log[m_1 - (0.6322 - 3.58 (b - y) + 5.20 (b - y)^2)]$$

for $0.22 \leq (b - y) < 0.375$, and:

$$[\text{Fe}/\text{H}] = -2.0965 + 22.45 m_1 - 53.8 m_1^2 - 62.04 m_1 (b - y) + 145.5 m_1^2 (b - y) + \\ (85.1 m_1 - 13.8 c_1 - 137.2 m_1^2) c_1 \quad (1)$$

for $0.375 \leq (b - y) \leq 0.59$. The average uncertainty for this calibration is stated to be $\Delta[\text{Fe}/\text{H}] = 0.16$ dex.

This calibration is applicable to the dwarf stars of spectral type ranging from F through early K which have been preferentially targeted in the radial velocity surveys. Rocha-Pinto & Maciel (1996) applied the Schuster & Nissen (1989) calibration to a sample of 79 G dwarfs in the solar neighborhood for which spectroscopic abundances have been determined, and found very good agreement across a wide range of metallicities. In particular, Rocha-Pinto & Maciel (1996) found that the Schuster & Nissen (1989) calibration shows better agreement with the spectroscopic abundances than does the calibration of Olsen (1984). In Figure 1, we compare *uvby* metallicities obtained by applying Equation 1 to the aggregate of planet-bearing stars for which alternate, mostly spectroscopic, determinations of the metallicities are available (see Butler et al. 2000 for references to individual determinations). For this high-metallicity subsample, the Schuster & Nissen (1989) calibration tends to *underestimate* the metallicity of a given star by an average of 0.06 dex in comparison to the spectroscopically determined value. We can thus conclude that the *uvby* calibration is sufficiently accurate for use in selecting a statistically metal-rich sample of stars from the Hauck & Mermilliod (1998) compilation.

The catalog shown in Table 2 was obtained with the following procedure. The database of Hipparcos target stars (Perryman et al. 1997) was queried for objects with (1) magnitudes in the range $7.8 < V < 11$, (2) parallaxes $\pi > 0.01$ arcseconds, and (3) color indices in the range $0.2 < B - V < 0.9$. This query yields a subset of 10,101 stars, most of which have HD identifiers. Within this subset, a second search was made for stars listed in the Hipparcos catalog as non-multiple and non-variable and which also appear in the Hauck & Mermilliod (1998) compilation. This cut yielded 4825 stars. $[\text{Fe}/\text{H}]$ estimates were then computed from each star’s *uvby* photometry. We find that 206 stars (4.27% of the sample) have $[\text{Fe}/\text{H}]$ values in excess of the Hyades metallicity of 0.125. Given the tendency of the Schuster & Nissen (1989) calibration to underestimate metallicity, these stars are quite likely to be very metal-rich, and, as such, should have an approximately tenfold increased probability (in comparison to field stars) of bearing short-period planets.

There are 31 stars in Table 2 with V magnitudes in the range $7.8 < V < 8.0$. Hence, as stated in Butler et al. (2000), they are thus likely to already be under radial velocity surveillance. Indeed, out of these 31 bright stars, eight are currently included in the Keck survey (Marcy, 2000 personal communication). Of these eight stars, one, (HD 187123) has a planet with $M \sin i = 0.54 M_{\text{JUP}}$ and a period of 3.097 days (Butler et al. 1998). One planet in eight stars is consistent with our expected occurrence rate of 10%.

We recommend that the stars in Table 2 be considered for targeting in planetary searches. The stars which are later than spectral type F5–F7 can be added to the radial velocity surveys currently underway, and all of the stars can be photometrically monitored for transits. In the next section, we describe a preliminary transit search of our catalog which makes use of the Hipparcos epoch photometry.

3. A Preliminary Search for Transiting Planets Among the High-Metallicity Catalog Stars

Given the frequency estimates in the introductory section, we expect that roughly 10% of the stars listed in Table 2 harbor short-period planets. Geometric arguments indicate that approximately 10% of short-period planets will display transits (Henry et al. 2000), so it is likely that there are 1–2 transiting planets orbiting stars in Table 2.

The roughly 10% fraction of short-period planets which exhibit transits are extremely useful. The orbital inclination of a transiting planet is determined to high accuracy, breaking the $\sin i$ degeneracy which plagues the radial velocity method of detection, and giving an unambiguous mass determination. A transit detection also yields a size and density for the planet. As more transiting planets are found, their distribution in the space delineated by mass, radius, and temperature will be instrumental in allowing for comparison with theoretical models. Each new transit will help to further unravel the structure and evolution of the extrasolar planets.

At present, only one transiting extrasolar planet is known. This object (HD 209458b) orbits its parent star with a period of 3.525 days, has a mass of $0.62M_{\text{JUP}}$, and a radius of $1.42R_{\text{JUP}}$. The parent star HD 209458 is a G0 main sequence dwarf with no known stellar-mass companions. Based on Hipparcos measurements of $V = 7.65$, $B - V = 0.594$, and $d = 47$ pc, Allende Prieto & Lambert (1999) estimate a mass of $1.03 M_{\odot}$, and a radius of $1.15 R_{\odot}$ for the star. HD 209458b was initially discovered with the radial velocity method (Henry et al. 2000, Mazeh et al. 2000). Subsequent measurements of the photometric light curve of the star revealed that the planet was transiting, with a transit duration of 3.1 hours, and a maximum transit depth of 1.6% (Henry et al. 2000, Charbonneau et al. 2000).

The primary mission of the Hipparcos satellite was to produce astrometric information. However, in addition to positional astronomy, the satellite also obtained an extensive database of photometric measurements during its 3.36 year mission. This Hipparcos epoch photometry (Perryman et al. 1997, van Leeuwen et al. 1997) covers 118,204 stars and contains an average of $n=110$ observations per star. Almost immediately after the announcement of the HD 209458 transit detection (Henry et al. 2000, Charbonneau et al. 2000) several authors demonstrated that the transit is visible in the Hipparcos epoch photometry (Söderjhelm 1999, Castellano et al. 2000, Robichon & Arenou 2000).

Figure 2 shows the 89 photometric measurements which the Hipparcos satellite made of HD 209458 (HIP 108859), folded at a period of 3.5247 days (consistent with the period obtained from the radial velocity observations). The error bars attached to the data points correspond to the quoted uncertainty of each individual measurement. The heavy solid line shows an approximation to the transit lightcurve in which the assumed transit depth is 1.6%, and the transit duration is 3 hours (see below). Note that the slopes of ingress and egress have been omitted. The transit is manifested as a rather unremarkable group of six measurements clustered around orbital phase 0.7. Castellano et al. (2000), however, have shown that with an *a priori* knowledge of the approximate

period, such a cluster of low points has approximately one chance in 5×10^4 of occurring by chance. Robichon & Arenou (2000) find a similar result, and suggest that additional transiting planets might be detectable within the Hipparcos epoch photometry. It is thus informative to carry out a preliminary search for the 1–2 transiting short-period planets that are expected to exist among the high metallicity stars in Table 2. This is especially true for stars of spectral type F6 and earlier which are inaccessible to radial velocity surveys (due to a lack of adequate spectral lines for velocity cross-correlations).

An automated routine was written to search for transiting planets in the Hipparcos photometry. For a particular star, the stellar mass and radius are estimated from the spectral type (see Allen, 2000). A hypothetical transiting planet is assumed to have a radius of $1.3 R_{\text{JUP}}$. This value is consistent with the observed radius of HD 209458b, and it agrees with theoretical expectations for the sizes of the so-called “Hot Jupiters”. In a study of the 51 Peg system, Guillot et al. (1996) used a detailed non-adiabatic structure model to show that the radii of 8 Gyr old planets in four day orbits exhibit a very narrow range of sizes varying from $1.2 R_{\text{JUP}}$ at $0.5 M_{\text{JUP}}$ to $1.4 R_{\text{JUP}}$ at $3.0 M_{\text{JUP}}$. Given the stellar properties and the radial size of the hypothetical transiting planet, we next choose a trial orbital period P . Transits are assumed to occur along the major chord of the star as seen from Earth. The orbital period is therefore sufficient to fix the transit duration, and the relative sizes of planet and star fix the transit depth, yielding an approximate light curve $y_p(\phi)$. The effects of limb darkening and transit ingress and egress are not considered. The large intrinsic scatter and the sparse sampling of the Hipparcos photometry obviates any benefit from these refinements.

For each star in Table 2, the Hipparcos photometry annex lists the observation epoch (referred to Julian day 2,440,000.0), the Hipparcos magnitude $H_p(i)$, the magnitude uncertainty $\sigma_H(i)$, and a data quality flag $f(i)$, for each photometric measurement (van Leeuwen et al. 1997). We reject data points for which $f(i) > 8$. The remaining n points are phased modulo the trial orbital period P . A chi-squared statistic

$$\chi^2(P, \phi_j) = \sum_{i=1}^n \left(\frac{H_p(i) - y_p(i, \phi_j)}{\sigma_H(i)} \right)^2 \quad (2)$$

is computed successively for 500 equally spaced trial transit phases ϕ_j spanning the range from 0 to 1, and the minimum chi-squared value is noted.

The procedure is then applied to 90,000 trial periods in the 1-10 day range, with $\Delta P = 0.0001$ days. Figure 3 shows $\chi_{\min}^2(P)$ for HD 209458, for periods in the subinterval ranging from three to four days. The correct transit period of 3.5247 days yields $\chi_{\min}^2(3.5247) = 115.57$, for a transit centered at phase $\phi = 0.704$. This value for χ^2 is the second-best fit to the data within the 3–4 day range. A spurious period of 3.7909 days yields a slightly lower value of $\chi_{\min}^2(3.7909) = 115.50$, and there is a third fit at 3.2952 days which is nearly as good.

The HD 209458 measurements (which are by no means atypical within the epoch photometry annex) indicate that unambiguous transit detections are not possible with typical Hipparcos data.

Nevertheless, the quality of the HD 209458 detection is high enough to warrant a survey of possible candidate events (period determinations) within the high metallicity catalog. The above-described procedure was applied to all 206 stars in Table 2, and periods with low chi-squared values were noted. These good-fit periods were then screened according to the several criteria chosen to enhance the likelihood of a period fit being a true detection. First, periods were required to fall in the range $3 < P < 4$ days. This period range is seemingly preferred by actual systems; as mentioned above, nearly half of the known short period planets fall in this one day interval. Second, only events with particularly low minima were chosen. Candidates are required to have unit weight error $u = \sqrt{\chi^2/n} < 1$. We also require that a candidate transit interval contain no more than 2.5 times the expected number of photometric measurements. In practice, particularly low chi-squared fits are often achieved by folding a large number of outlying points into a spurious transit interval. Nevertheless, true detections are enhanced by a lucky distribution of points. In the case of HD209485b, the six transiting points which contribute to the 3.5247 day period shown in Figure 3 are 2.25 times the number expected among 89 randomly distributed measurements. (Note that the Hipparcos photometric measurements are not distributed randomly in time. In many cases, successive measurements are either spaced very closely or interspersed with longer gaps than would be expected from a random distribution.) Candidate transits which meet these criteria are listed in Table 2. For these stars, we list (1) n , the number of acceptable photometric measurements for the star, (2) P , the best-fit period, (3) u , the unit weight error of the best chi-squared fit, and (4) $n_t/n_{expected}$, the ratio of observed to expected points in the transit interval. If multiple candidate periods are found for a particular star, only the period with the lowest chi-squared fit is listed. An example candidate transit detection is shown in Figure 4. The interested reader can examine other candidate transits in Table 2 by entering the Hipparcos identifier and the trial period into the folding algorithm featured at the Hipparcos website: <http://astro.estec.esa.nl/SA-general/Projects/Hipparcos/apps/PlotCurve.html>.

4. A Connection Between Metallicity and Stellar Mass for Planet-Bearing Stars

There appear to be two broad classes of explanation for the correlation between short-period planets and high stellar metallicity (see e.g. Gonzalez 1997). The first explanation posits that high metallicity parent clouds lead more readily to planet formation, and hence to a higher rate of occurrence of short-period planets. High values for Z mean that more rocky material is available in the nebula to form protoplanetary cores. Furthermore, the presence of nebular dust above a particular threshold may trigger vigorous planet formation. A possible explanation might proceed as follows: The paradigm scenario for the formation of planetesimals is that dust grains settle to the midplane of the disk where they become gravitationally unstable (Goldreich & Ward 1973). Within the last decade, however, it has been shown that turbulence driven by the vertical shear in the orbiting disk can prevent dust from settling into the thin layer required to activate gravitational instability (see Weidenschilling & Cuzzi 1993). Recently, however, Youdin & Shu (2000, private communication) have shown that inclusion of off-diagonal Brunt-Väisälä frequencies can

considerably reduce the effectiveness of the vertical shear in stirring up turbulence (see also Sekiya 1998). They find that if the dust density is more than twice the value expected in the minimum solar nebula, then the turbulence becomes ineffective for suppressing the Goldreich-Ward (1973) instability. Photoevaporation of a protostellar disk is one mechanism which can increase the dust-to-gas ratio to the required threshold, and a high metallicity nebula would require a smaller degree of photoevaporation to trigger instability, thus allowing for vigorous planet formation within the inner regions of a metal-rich disk.

The second hypothesis for the planet-metallicity correlation holds that systems which form short-period planets (independently of the initial metallicity) are also able to efficiently enrich their parent stars. The large observed metallicities therefore occur only in the convective envelope, and not within the star as a whole. This can occur by [1] complete inward migration of (metal-rich) planets onto the star in response to tidal interactions with the protostellar disk (Lin, Bodenheimer & Richardson 1996), [2] via the scattering of metal-rich planets onto the star (Rasio & Ford 1996), or [3] through the dumping of debris such as planetesimals, comets or asteroids onto the star (Murray et al. 1998, Quillen & Holman 2000).

Main sequence stars which are more massive than $\sim 0.25M_{\odot}$ and less massive than $\sim 1.4M_{\odot}$ have a radiative central core surrounded by a convective envelope. The more massive the star, the less mass is contained in the convective envelope. In the present day Sun, for example, the convection zone contains $0.02 M_{\odot}$ and extends over the outer 26% of the Sun’s radius (Sackmann, Boothroyd, & Kraemer 1993). The gas giant planets in our solar system appear to be enriched in heavy elements (partially as the result of their rock-ice cores), and are likely to have metallicities of order $Z \geq 0.1$. The dissolution of Jupiter (assuming $Z_{\text{JUP}} = 0.1$) into the convective envelope of the present day Sun would thus raise the metallicity of the convective envelope by 0.08 dex. By contrast, adding Jupiter to a $0.8 M_{\odot}$ ZAMS solar metallicity main sequence star, which has a $0.73 M_{\odot}$ convective envelope (Forestini 1994), yields a metallicity increase of only 0.025 dex. Folding Jupiter into the $0.007 M_{\odot}$ convective envelope of a $1.2 M_{\odot}$ ZAMS star gives a large metallicity increase of 0.176 dex.

Figure 5 indicates that there is some evidence for increasing metallicity with increasing stellar mass among all known planet-bearing stars for which metallicities are available. Most of the masses and metallicities shown in this plot were taken from Table 5 of Butler et al. (2000). Many of these metallicities result from spectroscopic determinations. In addition, four of the five new planet-bearing stars announced by Mayor et al. (2000), and the three new planet-bearing stars announced by Fischer et al. (2000) are also included. The planet-bearing stars HD 177830, GJ 876, and HD 83443 are not included in the figure, since neither high resolution spectroscopy nor *uvby* photometry is yet available for these stars. A linear regression to the data yields a best fit slope of $0.548 \text{ dex}/M_{\odot}$.

Stars which are heavier than roughly $1 M_{\odot}$ have main sequence lifetimes which are shorter than the age of the galactic disk. In general, therefore, a population of F dwarfs will be younger than a population of G dwarfs. For example, assuming a constant rate of star formation in the

Galaxy, and the stellar mass-lifetime relation given by Iben & Laughlin (1989), the average age of a sample of $1 M_{\odot}$ G dwarf stars is 4.15 Gyr, whereas the average age of an aggregate of $1.3 M_{\odot}$ F dwarf stars would be only 1.7 Gyr.

Edvardson et al. (1993) examined a sample of nearby F and G stars, and found that the average metallicity in their sample was a gradually decreasing function of age. Ng & Bertelli (1998) further quantified this relation, and found that the age-metallicity relation for the averaged population displays a small, but nevertheless discernable slope of 0.07 dex/Gyr. This result is in accordance with the enrichment of the galactic disk as a result of ongoing stellar evolution, and it means that a local sample of F dwarfs should be statistically more metal-rich than a similar sample of G dwarfs. Much of the enrichment, however, is reflected in the paucity of very metal-poor main sequence F stars.

We can check the degree to which the trend in Figure 5 is due to the younger average age of the F stars by constructing a local, volume-limited comparison sample of G, F, and early K dwarfs: We queried the Hipparcos catalog (Perryman et al. 1997) for all objects lying within 25 pc, and then removed the stars which are listed as either multiple (Hipparcos field H58 > 1) or variable. From this volume-limited subset, we retained all stars for which *uvby* measurements exist, and for which $0.22 < b - y < 0.59$. The masses of these stars were then obtained from the database of Prieto & Lambert (1998), and metallicities were computed using the Schuster & Nissen (1989) calibration. This yields an essentially complete, volume-limited sample of 196 G and F dwarfs which have metallicities in excess of $[\text{Fe}/\text{H}] = -0.4$, and masses in the range $0.88 M_{\odot} - 1.45 M_{\odot}$. These stars are plotted as open circles in Figure 6. For comparison, the metallicities of the planet-bearing stars were recomputed using the Schuster & Nissen (1989) calibration) and plotted as filled circles. As mentioned in Butler et al. (2000), most of the mass estimates for the planet-bearing stars in Figure 5 are from the Prieto & Lambert (1998) database, so a comparison of $[\text{Fe}/\text{H}]$ vs. M for the two populations is readily justified.

The use of the Schuster & Nissen (1989) calibration in Figure 6 maintains a noticeable metallicity-mass gradient among the planet-bearing stars of 0.498 dex/ M_{\odot} , yet there is only a marginal -0.064 dex/ M_{\odot} gradient among the stars in the local sample with $[\text{Fe}/\text{H}] > -0.4$. This nearly null slope for the local aggregate is in good agreement with the conclusion of Rocha-Pinto & Maciel (1998), who find that there is a “remarkable consistency amongst the [metallicity] distributions of F, G, and K type dwarfs.”

Furthermore, Figure 6 shows that for $M < M_{\odot}$, the planet-bearing stars are drawn essentially randomly from the metallicity distribution of stars having $[\text{Fe}/\text{H}] > -0.4$. By $1.2 M_{\odot}$, however, the planet-bearing stars lie in the region occupied by the most metal-rich stars of the local distribution. The two planet-bearing stars with $M \geq 1.4 M_{\odot}$ (HD 38429 and HD 89744) are more metal-rich than any star of similar mass within 25 pc.

As a general trend, solar-type stars begin their pre-main-sequence evolution on the Hayashi track with a fully convective stellar configuration. After several million years, radiative cores appear

and the size of the convective envelope steadily decreases over the next 10 million years or so. The lifetimes of protostellar disks are on the order of several million years. As discussed by Laughlin & Adams (1997), if planets are added to the star primarily as a result of inward migration caused by tidal interactions between the disk and its embedded planets, then a metallicity gradient as a function of stellar mass is likely to exist only among early F-type and A-type stars ($1.5 - 2.5 M_{\odot}$). Stars in this mass range have relatively low-mass convective envelopes during the phase when a protoplanetary disk is present. Laughlin & Adams (1997) examined the metallicities of a volume-limited sample of F dwarfs, and found only marginal evidence for such a trend. If the much more dramatic trend shown in Figure 5 among the K-type through late F-type type planet-bearing stars is real, then the enrichment processes must be occurring over timescales which are considerably longer than the typical disk lifetime. The long-term process of resonant scattering of planetesimals into the parent star would thus provide the most natural mechanism for enrichment.

5. Using Binary Stars to Probe the Metallicity Correlation

Short-period binary stars can provide another observational test to select between the initial metallicity hypothesis and the enrichment hypotheses. The basic idea is straightforward. A close binary star, once formed, will tend to protect itself against accretion of either planets or other debris. Material which wanders within several binary separations of the central stars tends to be ejected from the system as a result of three-body interactions.

As a first illustration of this principle, one can imagine a circumbinary disk which has formed a Jupiter-mass planet. Tidal interactions between the disk and the planet are then imagined to cause the planet to migrate inwards towards the central binary star. This process can be simulated by placing Jupiter-mass particles in 2 AU circular orbits around the center of mass of a 0.25 AU zero-eccentricity binary with equal component masses of $0.5 M_{\odot}$. The tidal effect of the circumbinary disk is modeled as a tiny, constant azimuthal torque which causes the planetary orbit to spiral inward on a 10^5 year timescale. Once the orbit has decayed to the point where the planet reaches an orbital radius of several binary separations, 3-body interactions tend to eject the planet from the system. A typical example of this process is illustrated in Figure 7.

Using a Bulirsch-Stoer integration scheme, we have computed 400 different simulations of inward planetary migration onto the binary star system described above. Variations in the initial conditions were obtained simply by varying the initial orbital phase of the Jupiter-mass planet in its 2 AU circular orbit. We find that in 356 cases (89% of the time), the planet is ejected from the system. We found that 23 of the simulations resulted in the planet colliding with the first star, and that 21 of the simulations ended in collision with the second star. As we discussed above, if the mass-metallicity trend shown in Figures 5 and 6 continues to hold as more planets are discovered, then it is rather unlikely that the planet – stellar metallicity correlation results from accretion of planets during the phase when a gaseous protostellar disk is present. However, if accreting planets really are responsible for the metallicity trend, it is clear that close binary stars can eject

most planets which migrate into their vicinity, and one would expect a deficit of super-metal-rich spectroscopic binaries, especially among the easily enriched A and F type stars.

Once the gaseous nebula has dispersed, enrichment of the convective envelope can occur as long-term dynamical instabilities among the planets, planetesimals and debris still present in the system cause material to be cast onto the fully formed star. Again, however, close binaries should be more adept than single stars at keeping such material at bay.

To illustrate how binary self-protection works in the longer-term context of resonant scattering, we have computed two sets of long-term integrations of a simplified model of a planetary system. In the first set of integrations, two planets are placed in orbit around a solar mass star. The inner planet is given a semi-major axis $a = 5AU$, and an eccentricity $e = 0.05$. The planetary mass is assumed to be $1.0 \times 10^{-3}M_{\odot}$. These parameters are quite close to the present day properties of Jupiter. The second planet is given a mass of $6.0 \times 10^{-4}M_{\odot}$, an eccentricity $e = 0.1$, and a semi-major axis $a = 9AU$. These values were chosen in order to yield a system which is similar to, but dynamically slightly more active than our own Jupiter-Saturn pair.

256 test particles were placed on circular orbits around the central star, with initial semi-major axes ranging in equally spaced increments from 1.0 to 3.6 AU. The system was then integrated forward in time for one million years using a Bulirsch-Stoer integration scheme (Press et al. 1996). The eccentricities and semi-major axes of the test particles were frequently evaluated. In Figure 8, the maximum eccentricity achieved by each particle is indicated by an open circle plotted with respect to the initial semi-major axis.

Figure 8 indicates that many orbital trajectories within the two planet model system suffer large increases in eccentricity. The broad resonant feature centered at approximately 2.1 AU is the analog of the ν_6 secular resonance in the Solar System. This resonance arises because the induced precession rates of the perihelia of the test particles in this region are commensurate with the precession of the perihelion of the outer saturn-like planet (see e.g. Murray & Dermott 1999). Powerful resonances of this sort are expected to be common when a system contains more than one giant planet. Other resonance features are also visible. At 3.15 AU, for example, the 2:1 mean motion resonance with the inner Jupiter-mass planet leads to a significant eccentricity increase for the particles having initial semi-major axes that place them in this region.

Particles which find themselves in strong resonances such as the ν_6 rapidly develop very large eccentricities. In many calculations, the eccentricity grows so large that the perihelion, $r_p = a(1 - e)$, of the particle is smaller than the stellar radius. When this situation occurs, the object is destroyed by the star, and its burden of heavy elements is mixed through the convective envelope (see Quillen & Holman 2000). Alternately, some particles which develop extreme eccentricities also experience increases in semi-major axis which cause their orbits to cross the orbits of the planets. In such cases, the particles are often ejected from the system without encountering the central star. In Figure 8, the particles which crash into the central star are indicated by filled black circles. The wide ν_6 resonance is seen to be the most effective mechanism for delivering debris to the surface of

the central star.

Figure 8 also shows the results of integrations in which the same system of two planets was started in circumbinary orbit around a pair of $0.5 M_{\odot}$ stars on an $e=0.0$ orbit of separation $a = 0.25$ AU. A total of 220 test particles were placed on circular orbits in the region between 1.5 and 3.8 AU. In this alternate system, the strong high-frequency perturbation arising from the binary potential destroys or weakens many of the resonances. In particular, the ν_6 resonance, which efficiently directed material onto a single central star, is now completely absent. Furthermore, those particles which do receive large eccentricities tend to suffer close encounters with the perturbing planets and are ejected from the system without encountering the central stars, and the small fraction of particles that do manage to find themselves in the vicinity of the central stars stand a high probability of being ejected. Out of the 220 test particles in the simulation, none were observed to hit either member of the binary pair.

The foregoing calculations are by no means exhaustive or definitive, but the suggestion is clear. A close binary star is capable of protecting itself against enrichment. If enrichment is responsible for the enhanced metallicity of planet-bearing stars, then there should be a statistical deficit of super-metal-rich short period binary systems.

Can such a statistical deficit be observed? For spectroscopic binary stars, individual double lines will represent an added technical difficulty for spectroscopic determinations of the metallicity. One must separate the composite spectrum into two spectra corresponding to the individual stars. There have been some attempts to obtain metallicities for double-lined eclipsing spectroscopic binaries in order to make the eclipsing systems a better test of stellar evolution models (e.g. Ryabchikova et al. 1999). However, there are not yet enough determinations to constitute a statistically meaningful sample, and the metallicities which have been obtained are not as accurate as for single stars (G. Gonzalez, personal communication).

If the two binary components are of the same spectral type (as would be the case in the system used for our test integrations) then *uvby* photometry gives a meaningful metallicity estimate if one assumes that the metallicities of both stars are the same. Alternately, for systems with extreme mass ratios – an F8, say, and an M8 – where the flux from the secondary is swamped by the flux from the primary, it should be possible to get a determination of the metallicity of the primary component either with a spectroscopic analysis or with *uvby* photometry. In any case, a comprehensive survey of metallicities of close binary systems would be a very valuable resource.

6. Discussion

We have studied the emerging correlation between high stellar metallicity and the presence of extrasolar planets. This correlation is one of several unexpected and exciting results which have stemmed from the growing census of extrasolar planets. Our results are summarized as follows:

1. The frequency of occurrence of short-period planets (those with periods $P < 20$ days) is approximately 1% among solar type stars. Among the most metal-rich stars ($[\text{Fe}/\text{H}] > 0.2$) this fraction increases to approximately 10%.

2. Metallicity estimates using the Schuster & Nissen (1989) calibration of *uvby* photometry yield $[\text{Fe}/\text{H}]$ values which are well correlated with metallicities derived from detailed spectroscopic analysis (see Figure 1). The *uvby* calibration, however, systematically underestimates metallicities by ~ 0.06 dex for stars of solar metallicity and above.

3. Using the Hipparcos database (Perryman et al. 1997), and the Hauck & Mermilliod (1998) listing of *uvby* photometry, we have compiled a catalog of 206 metal-rich stars which are dim enough ($V > 8$) to have likely eluded inclusion in the current radial velocity surveys (Table 2). We advocate that these stars be added to ongoing surveys, due to their high likelihood of possessing short-period planets. It is important to locate more short-period planets in order to be assured of further transiting systems. Transits are very important because they allow planetary properties (mass, radius, density) to be uniquely determined. We should mention, however, that the new systems discovered within this candidate list should not be used in future statistical analyses of the incidence rate of planets discovered with the Doppler method.

4. We have used the Hipparcos epoch photometry to carry out a search for transiting planets associated with the stars in our high-metallicity catalog. We show that in the absence of *a priori* information regarding the period, the quality of the Hipparcos photometry is insufficient to make unambiguous detections. The data quality is, however, high enough to identify candidate events (see for example Figure 4), and we have listed a number of candidate periods associated with the stars in our catalog.

5. There is a preliminary suggestion of a trend toward increasing metallicity with increasing stellar mass among the aggregate of known planet-bearing stars (Figure 5). This trend is consistent with a scenario in which systems capable of forming short-period planets are also capable of enriching the convective envelopes of their parent stars after the gaseous protoplanetary disks have dispersed. As shown by Figure 6, the trend does not appear to stem from the systematic differences in age between F and G stars.

6. We have explored the possibility of using spectroscopic binary stars to determine the underlying cause of the extrasolar planet – stellar metallicity correlation. If the large stellar metallicities are due to a post-formation enrichment process, then super-metal-rich spectroscopic binaries should be rare in comparison to their single counterparts.

As more planets are discovered, the true extent of the correlations discussed here will become evident. In particular, it will be interesting to see whether the correlation continues to hold for systems like our own, in which the Jovian-mass planets have orbital periods of a decade or longer. Such systems, if they are common, will soon be uncovered by the radial velocity surveys.

The work in this paper represents a first effort to exploit the planet – metallicity connection,

and hence there is a great deal of additional interesting research which could be done. For example, it would be worthwhile to search the brightest early F dwarfs in the Hipparcos database for transits. The early F dwarfs are inaccessible to planet detection via the radial velocity method, and have not yet been monitored for planets. These stars, however, have considerably smaller relative errors in their photometric measurements, and are hence considerably better suited to transit detection than the dim stars analyzed in Table 2. The dynamical calculations in this paper would benefit from a wider survey of parameter space in order to better quantify the ability of close binary stars to protect themselves against enrichment. Additionally, as discussed in section 5, it will be very useful to obtain the metallicities of a statistically significant sample of spectroscopic binary stars.

The existence of a connection between high stellar metallicity and the presence of a short-period planet is one of the most exciting developments that has accompanied the discovery of extrasolar planets. This remarkable correlation is telling us something profound about the formation and evolution of planetary systems.

6.1. Acknowledgements

I would like to thank Fred Adams, Douglas Caldwell, Tim Castellano, John Chambers, Debra Fischer Guillermo Gonzalez, Geoff Marcy, Doug Lin, & Andrew Youdin for discussions which made this work possible. Guillermo Gonzalez provided a helpful referee’s report, which led to the inclusion of Figure 6 in the manuscript. This research has made use of the SIMBAD database, operated at CDS, Strasbourg, France. This work was supported by a NASA astrophysics theory program which supports a joint Center for Star Formation Studies at NASA-Ames Research Center, UC Berkeley and UC Santa Cruz.

REFERENCES

- Allende Prieto, C., & Lambert, D. L. 1999, *AA*, 352, 555
- Cox, A. N. 2000, *Allen’s Astrophysical Quantities* (AIP Press Springer: New York)
- Bodenheimer, P., Hubickyj, O., & Lissauer, J. L. 2000, *Icarus*, 143, 2
- Borucki, W. J., Koch, D. G., Dunham, E. W., & Jenkins, J. 1997, in *ASP Conf. Ser. 119, Planets beyond Our Solar System and the Next Generation of Space Missions* (San Francisco: ASP), 153
- Brown, T. M. et al. 2000, *BAAS*, 19, 203
- Butler, R. P., Marcy, G. W., Williams, E., Hauser, H., & Shirts, P. 1997, *ApJ*, 474, L115
- Butler, R. P., Marcy, G. W., Vogt, S. S., & Apps, K. 1998, *PASP*, 110, 1389

- Butler, R. P., Vogt, S. S., Marcy, G. W., Fischer, D. A., Henry, G. W., & Apps, K. 2000, *ApJ* In Press (to appear Dec 1 2000).
- Castellano, T., Jenkins, J., Trilling, D. E., Doyle, L., & Koch, D. 2000, *ApJ*, 532, L51
- Castro, S., Rich, R. M., Grenon, M., Barbuy, B., & McCarthy, J. K. 1997, *AJ*, 114, 376
- Charbonneau, D., Brown, T. M., Latham, D. W., & Mayor, M. 2000, *ApJ*, 529, L49
- Edvardsson, B., Anderson, J., Gustafsson, B., Lambert, D. L., Nissen, P. E., & Tomkin, J. 1993, *AA*, 275, 101
- Fischer, D. A., Marcy, G. W., Butler, R. P., Vogt, S. S., Frink, S. F., Apps, K. 2000 *ApJ*, submitted
- Giménez A. 2000, *AA*, 356, 213
- Gliese, W. & Jahreiss, H. 1991, *Third Catalogue of Nearby Stars*. Astron. Rechen-Inst. Heidelberg
- Goldreich, P., & Ward, W. R. 1973, *ApJ*, 183, 1051
- Gonzalez, G. 1997, *MNRAS*, 285, 403
- Gonzalez, G. 1998, *AA*, 334, 221
- Gonzalez, G. 1999, *MNRAS*, 308, 447
- Gonzalez, G., Wallerstein, G., & Saar, S. H. 1999, *ApJ*, 511, L111
- Gonzalez, G. 2000, *ASP Conf. Ser.* (in press), *Disks, Planetesimals, and Planets*, ed. F. Garzon, C. Eiroo, D. de Winter & T. J. Mahoney, (San Francisco: ASP)
- Guillot, T., Burrows, A., Hubbard, W. B., Lunine, J. I., & Saumon, D. 1996, *ApJ* 459, L35
- Hauck, B. & Mermilliod, M. 1998, *AAS*, 129, 431
- Henry, G. W., Marcy, G. W., Butler, R. P., & Vogt, S. S. 2000, *ApJ*, 529, L41
- Holman, M., Touma, J., & Tremaine, S. 1997, *Nature*, 386, 254
- Hut, P. 1981, *AA*, 99, 126
- Iben, I. Jr. & Laughlin, G. 1989, *ApJ*, 341, 312
- Koch, D. G., Borucki, W. J., Webster, L., Dunham, E., Jenkins, J., Marriott, J., & Reitsema, H. 1998, *Proc. SPIE*, 3356, 599
- Laughlin, G. & Adams, F.C. 1997, *ApJ*, 491, L51
- Laughlin, G. & Adams, F.C. 1998, *ApJ*, 508, L171

- Lin, D. N. C., Bodenheimer, P., & Richardson, D. C. 1996, *Nature*, 380, 606
- Levison, H.F., Lissauer, J.J., & Duncan, M. J. 1998, *AJ*, 116, 1998.
- Marcy, G. W., & Butler, R. P. 1998, *ARAA*, 36, 57
- Marcy, G.W., Cochran, W.D. & Mayor, M. 2000, in *Protostars and Planets IV*, ed. V. Mannings, A. P. Boss & S. S. Russell (Tucson: University of Arizona Press), p.1285.
- Mayor, M., & Queloz, D. 1995, *Nature*, 378, 355
- Mayor, M., Naef, D., Pepe, F., Queloz, D., Santos, N. C., & Udry, S. 2000, <http://obswww.unige.ch/~udry/planet/planet.html>
- Mazeh, T. et al. 2000, *ApJ* 532, L55
- Murray, C. D. & Dermott, S. F. 1999, *Solar System Dynamics* (Cambridge University Press, Cambridge).
- Murray, N., Hansen, B., Holman, M., & Tremaine, S. 1998, *Science*, 279, 69
- Ng, Y. K. & Bertelli, G. 1998, *AA* 329, 943
- Olsen, E. H. 1984, *AASS*, 57, 443
- Perryman, M.A.C., et al. 1997, *The Hipparcos Catalog*, *A&A*, 323, L49
- Press, W. H., et al. 1992, *Numerical Recipes: The Art of Scientific Computing* (Cambridge: Cambridge Univ. Press)
- Quillen, A. C., & Holman, M. 2000, *AJ*, 119, 397
- Rasio, F. A., & Ford, E. B. 1996, *Science*, 274, 954
- Rocha-Pinto, H. J., & Maciel, W. J., 1996, *MNRAS*, 279, 447
- Rocha-Pinto, H. J., & Maciel, W. J., 1999, *AA*, 339, 791
- Robichon, N., & Arenou, F. 2000, *AA*, 255, 295
- Ryabchikova, T. A., Malanushenko, V. P., & Adelman, S. J. 1999, *AA*, 351, 963
- Sackmann, I.-J., Boothroyd, A. I., & Kraemer, K. E. 1993, *ApJ*, 418, 457
- Sandquist, E., Taam, R. E., Lin, D. N. C., & Burkert, A. 1998, *ApJ*, 506, L65
- Schuster, W. J., & Nissen, P. E. 1989, *A&A*, 221, 65
- Sekiya, M. 1998, *Icarus*, 133, 298

- Söderhjelm, S. 1999, *Information Bulletin on Variable Stars*, 4816, 1
- van Leeuwen, F., Evans, D. W., Grenon, M., Grossmann, V., Mignard, F., & Perryman, M. A. C. 1997, *AA*, 323, L61
- Vogt, S. S., Marcy, G. W., Butler, R. P., & Apps, K. 2000, *ApJ*, 536, 902
- Weidenschilling, S. J., & Cuzzi, J. N. 1993, in *Protostars and Planets III*, ed. (Tucson: University of Arizona Press) p. 1031
- Wisdom, J. 1983, *Icarus*, 56, 51

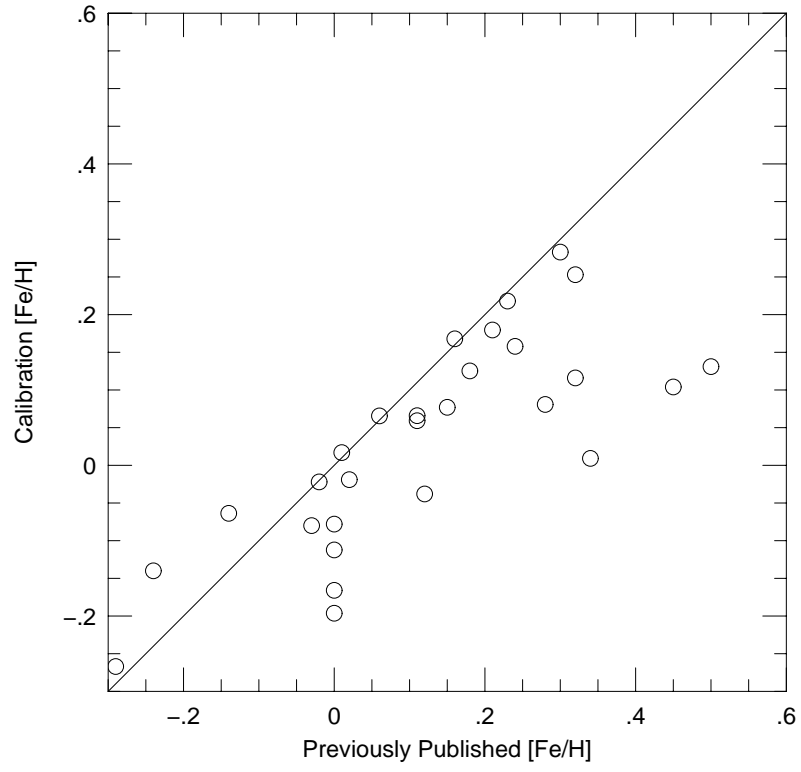


Fig. 1.— *uvby* metallicities for planet-bearing stars obtained with the Schuster & Nissen (1989) calibration in comparison with previously determined metallicities compiled by Butler et al. 2000.

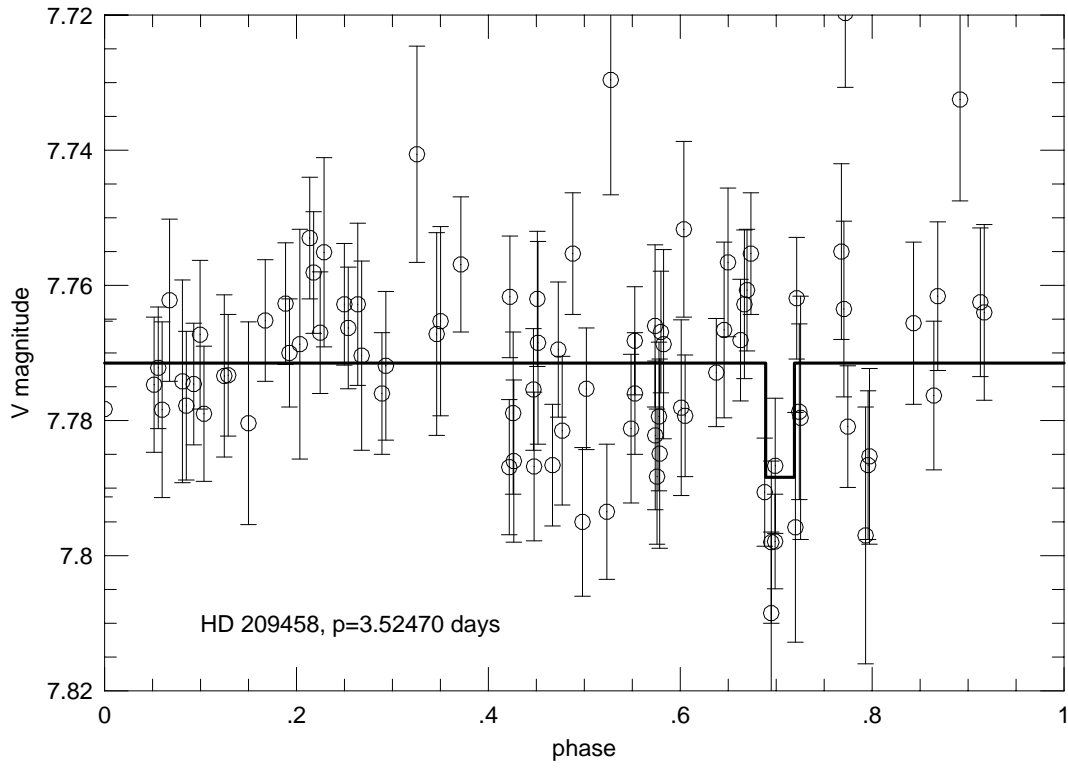


Fig. 2.— 89 measurements from the Hipparcos epoch photometry for HD 209458, folded at a period of 3.5247 days. An idealized transit lightcurve for the planet is shown.

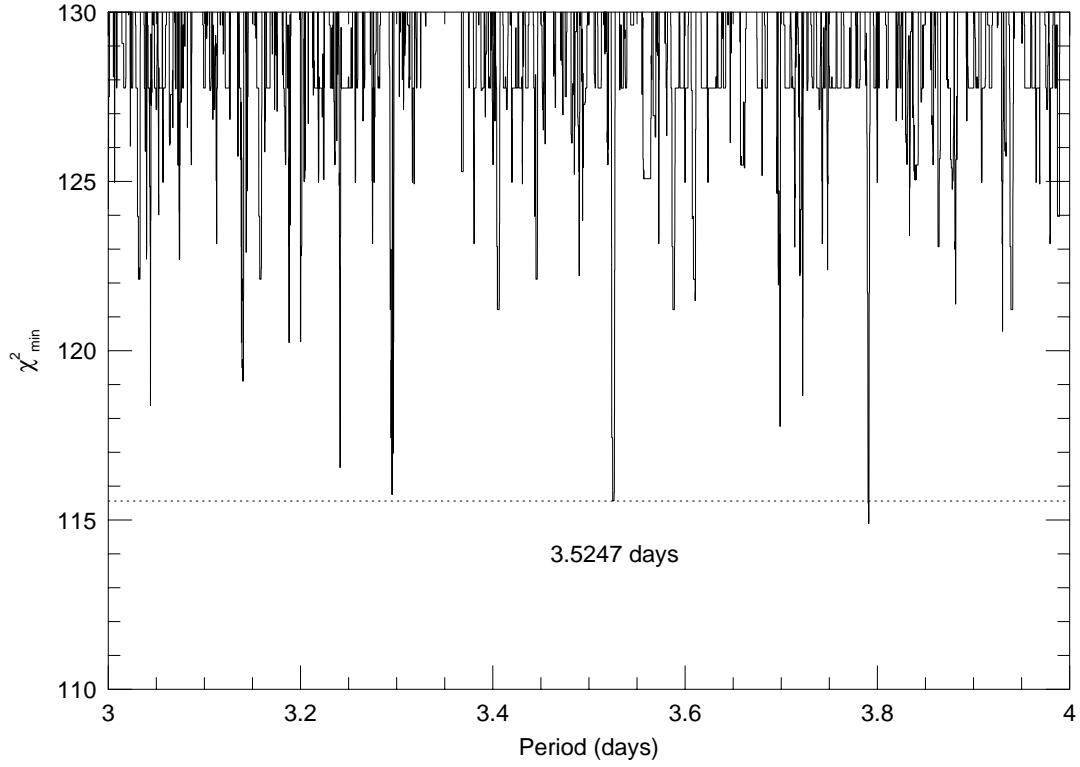


Fig. 3.— Minimum χ^2 fits to the Hipparcos epoch photometry for HD 209458. The true detection at period $P=3.5247$ days is indicated, and the level of the corresponding minima is indicated by the dashed line. Note that a spurious transit interval of $P=3.7909$ days has a slightly lower χ^2 fit to the aggregate of photometric measurements.

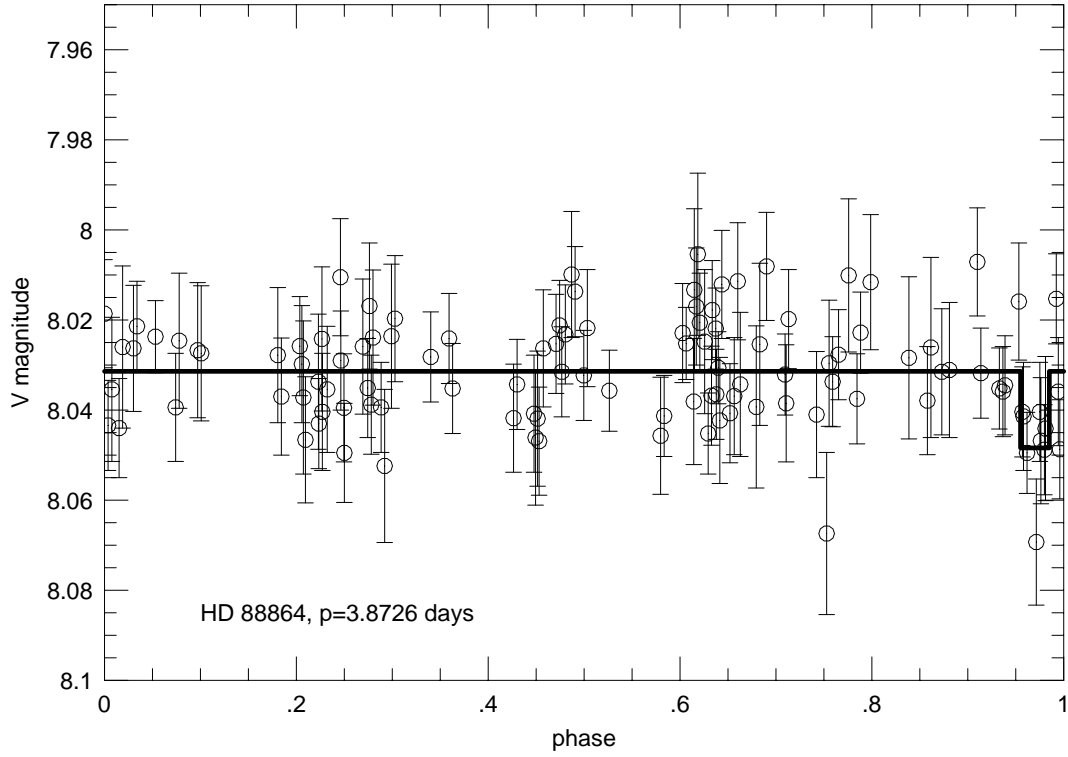


Fig. 4.— Hipparcos epoch photometry for HD 88864, folded at a period of 3.8726 days. There are 114 photometric observations. The lightcurve of a transit candidate event is shown. HD 88864 is an F8V star with a *uvby* metallicity $[\text{Fe}/\text{H}]=0.235$.

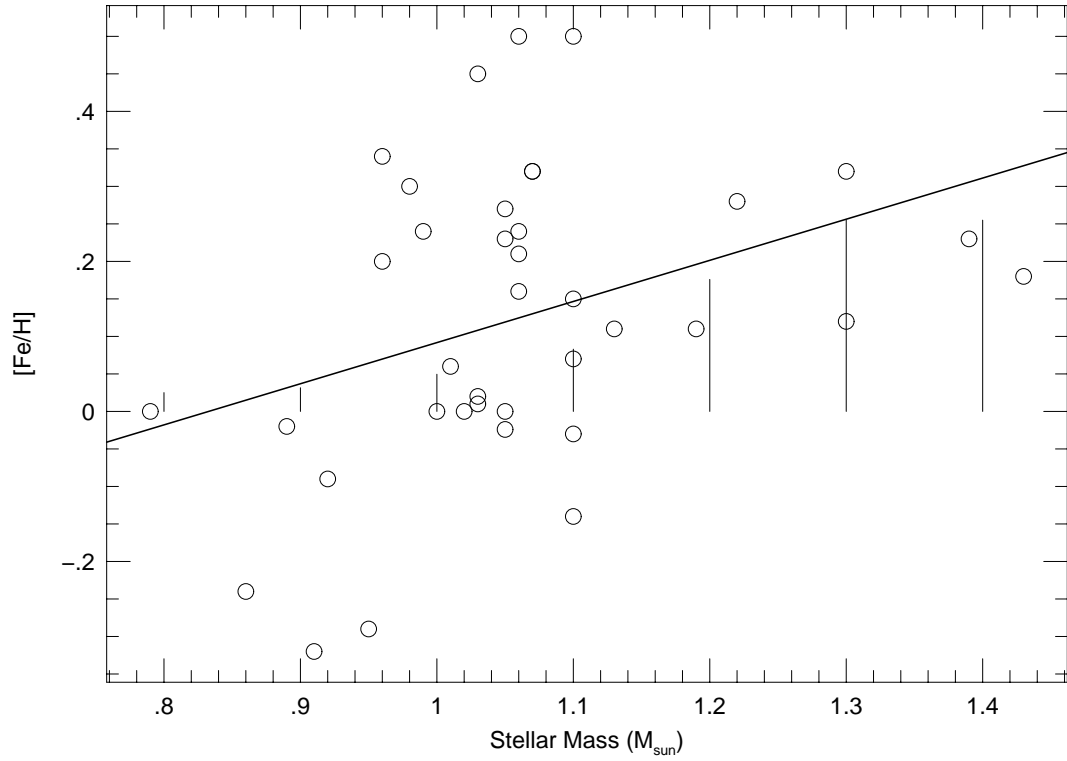


Fig. 5.— Metallicity vs. Stellar Mass for the known planet-bearing stars. A best-fit slope to the data is shown, illustrating a possible trend toward increasing metallicity as a function of stellar mass among the stars plotted. The increase in metallicity achieved by adding $30 M_{\oplus}$ of heavy elements to the convective envelopes of various stars of solar metallicity are shown as vertical lines whose height corresponds to the metallicity increase. The $30 M_{\oplus}$ of debris added to the fully radiative $1.4 M_{\odot}$ star is assumed to mix with $0.004 M_{\odot}$ of the stellar envelope.

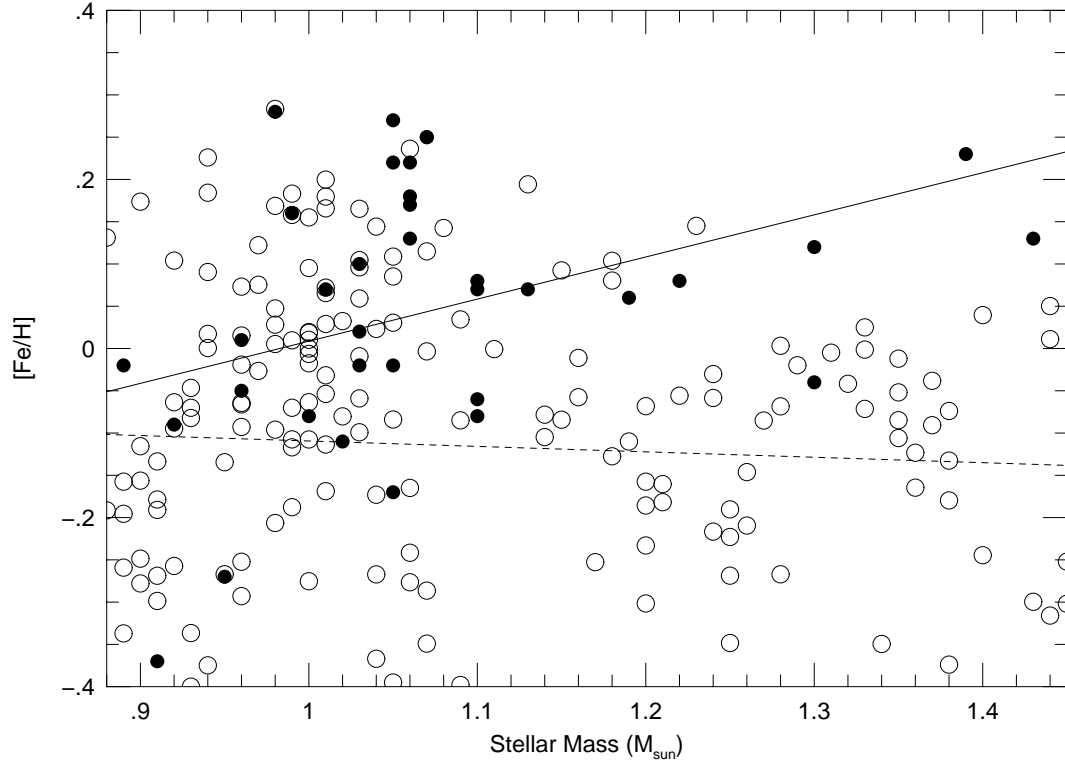


Fig. 6.— Metallicity vs. Stellar Mass for a volume-limited sample of nearby stars with $M > 0.88M_{\odot}$ and metallicity $[\text{Fe}/\text{H}] \geq -0.4$ (open circles). A best-fit slope through the data is shown as a dashed line. Also shown are the *uvby* metallicities of the known planet-bearing stars (filled circles). A best-fit slope to this data is shown as a solid line.

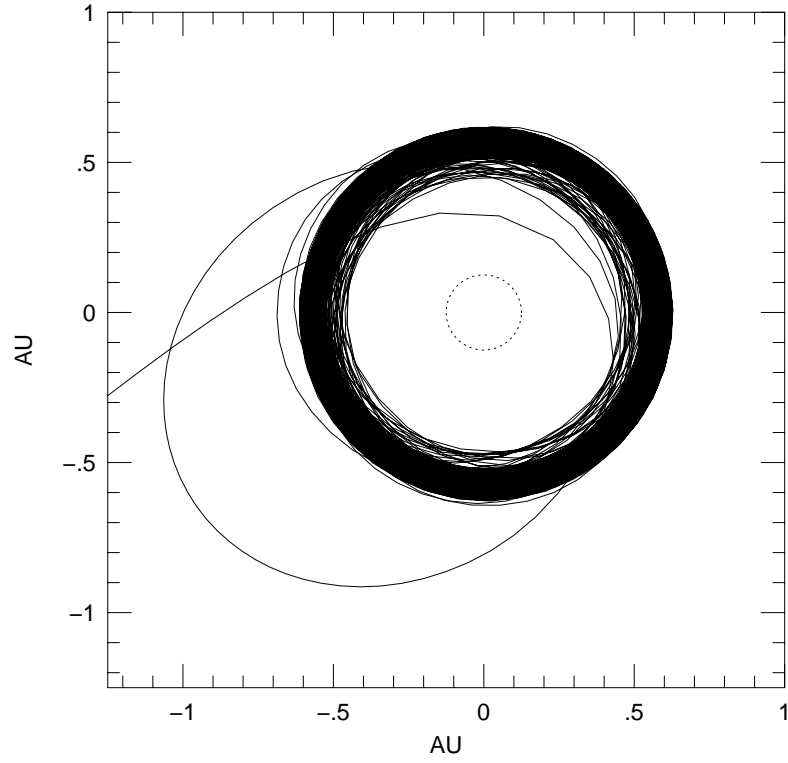


Fig. 7.— Illustration of a three-body encounter leading to ejection of a planetesimal from a binary system. The orbit of the equal mass, $e = 0$. central binary is shown as the dashed central circle. The trajectory of a test particle placed in orbit around the binary center of mass (and subjected to a small, constant azimuthal torque) is shown by a thin solid line.

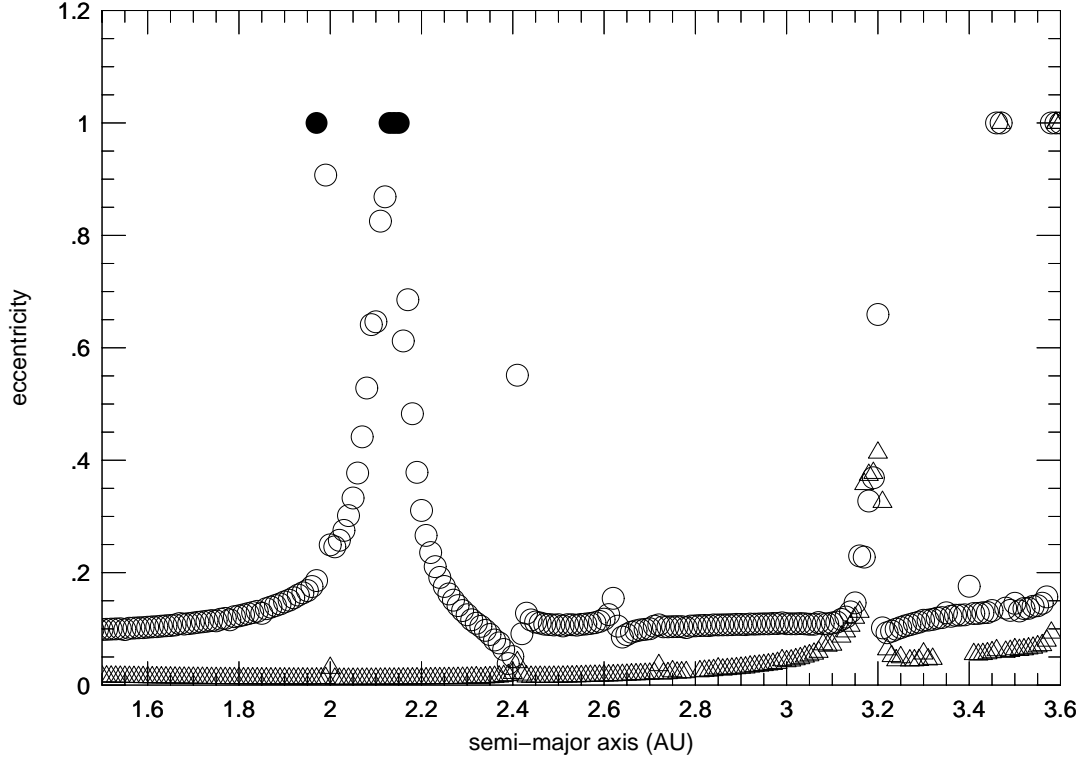


Fig. 8.— Maximum eccentricity of test particles placed in a model planetary system with two planets and (a) a single central star, and (b) a central binary with eccentricity $e=0$. and separation $a=0.25$ AU. Circles show the maximum eccentricities obtained for particles placed on circular orbits with a range of initial semi-major axes. Ejections are shown as open circles with $e=1$. Collisions with the central star are shown as filled circles. The triangles show the maximum eccentricities (with respect to the center of mass) of particles placed in circumbinary orbits over a range of semi-major axes. Ejections are shown as open triangles with $e=1$. No collisions with the central stars occurred in the circumbinary simulations.

Table 1
Short Period Planets and their Parent Stars

Star	Spectra	Period	e	$M \sin(i)$	[Fe/H]
HD83443	K0V	2.986	0.00	0.30	—
HD46375	K1IV – V	3.024	0.00	0.24	0.34
HD187123	G3V	3.097	0.01	0.54	0.16
HD120136	F7V	3.313	0.02	4.14	0.32
BD – 103166	G4V	3.487	0.05	0.48	0.50
HD75289	G0V	3.508	0.00	0.46	0.28
HD209458	G0V	3.524	0.02	0.63	0.00
HD217014	G2V	4.231	0.01	0.46	0.21
HD9826	F8V	4.617	0.02	0.68	0.12
HD168746	G5	6.400	0.00	0.24	–0.09
HD217107	G7V	7.130	0.14	1.29	0.30
HD108147	F8/G0V	10.88	0.56	0.30	–0.02
HD130322	K0V	10.72	0.05	1.15	–0.02
HD38529	G4IV	14.30	0.27	0.77	0.23
HD75732	G8V	14.66	0.03	0.93	0.45
HD13445	K1V	15.80	0.04	4.23	–0.24
HD195019	G3V	18.20	0.01	3.55	0.00

Table 2
A Catalog of Metal-Rich Stars

HIP#	HD#	Type	V	d	[Fe/H]	n	P	χ^2	n_t/n_{ex}
3391	4113	G5V	7.99	44.05	.159				
6978	9070	G5	8.00	42.74	.321				
9035	11833	G0	8.00	87.18	.148				
15005	20155	G0V	7.95	93.46	.131				
19148	25825	G0	7.88	46.71	.133				
20723	28185	G5	7.88	39.56	.150				
30860	45350	G5	7.96	48.95	.190				
32161	48458	F3V	7.88	95.06	.185				
38127	64141	F2IV	7.93	96.15	.197	106	3.5533	.939	1.29
40761	69809	G0	7.93	50.58	.140	92	3.0658	.971	.61
44137	76909	G5	7.92	47.66	.221				
46324	81659	G6/G8V	7.97	39.89	.130				
50020	88864	F8V	7.97	92.76	.235	114	3.8726	.873	2.04
51257	90711	K0V	7.94	32.13	.174	80	3.1836	.861	1.96
51258	90722	G5/G6IV	7.96	50.74	.271				
51579	91204	G0	7.89	51.76	.171	89	3.1787	.896	2.26
52939	93849	G0/G1V	7.92	74.07	.240	154	3.5060	.909	1.79
53537	94835	G0	7.99	49.46	.151				
55464	98727	F7V	7.91	68.17	.187	65	3.7355	.998	1.31
57345	102165	F7V	7.88	85.40	.360	102	3.6098	.921	1.36

HIP#	HD#	Type	V	d	[Fe/H]	n	P	χ^2	n_t/n_{ex}
59572	106156	G8V	8.00	30.96	.149				
60753	108351	F7V	7.96	88.11	.306	116	3.7653	.852	.74
61044	108942	G5	7.99	47.57	.156				
66749	118984	F3V	7.93	93.28	.400	100	3.7593	.877	2.28
81347	149724	G5	7.92	55.77	.178	94	3.2479	.920	2.17
81767	150437	G5V	7.92	55.13	.187	50	3.6016	.830	2.50
85017	157172	G8V	7.94	33.48	.143				
97336	187123	G5	7.92	47.92	.168				
104367	201203	F8/G0V	7.95	91.32	.183	57	3.5761	.908	1.45
109836	211080	G0	7.89	81.37	.162	56	3.1948	.860	2.06
111486	213401	G5IV/V	7.97	67.52	.134				
112187	215192	F2	7.97	97.47	.167	92	3.5231	.971	1.78
5529	7199	K0IV/V	8.12	35.88	.126				
10492	13945	G6IV	8.15	43.37	.139				
10599	13997	G5	8.06	34.07	.141	68	3.2407	.896	2.14
16405	21774	G5	8.15	49.90	.163				
28395	40590	F6V	8.15	85.91	.148	80	3.3677	.886	1.65
31895	48265	G5IV/V	8.14	87.41	.175	98	3.2525	.748	1.19
32916	49674	G0	8.18	40.73	.225				
36993	60521	G0	8.06	51.92	.129				
38104	62923	G5	8.13	51.47	.159				
40411	68659	F2	8.05	96.25	.200				
41022	69960	G5	8.08	61.20	.130				
42214	73256	G8/K0V	8.15	36.52	.127				
45406	79498	G5	8.11	48.64	.199	78	3.9984	.824	2.14

HIP#	HD#	Type	V	d	[Fe/H]	n	P	χ^2	n_t/n_{ex}
49060	86680	G0V	8.05	99.70	.262				
58813	104760	G2/G3III	8.09	55.68	.262				
59382	105844	G5	8.14	42.90	.147				
60081	107148	G5	8.09	51.26	.253				
62583	111431	G3V	8.09	83.61	.227	86	3.5510	.839	1.44
81421	149933	G5	8.12	37.65	.143				
91332	171918	G0	8.06	57.64	.277				
94625	179699	F8/G0V	8.08	79.94	.141				
94718	180556	F8	8.16	76.10	.196	121	3.0382	.937	1.02
99727	192343	G4V	8.09	65.83	.773	81	3.1428	.973	2.46
103692	200078	G5	8.13	52.69	.157				
104903	202206	G6V	8.15	46.34	.236	137	3.6257	.987	.92
105906	205521	G5	8.13	46.99	.199				
106006	204313	G5V	8.09	47.30	.130				
109169	211681	G5	8.17	70.87	.144	127	3.0527	.921	1.54
3488	4333	F5V	8.17	81.23	.243				
5189	6558	F8	8.27	73.75	.137	88	3.7859	1.000	1.62
6712	8765	G5	8.22	75.13	.196	88	3.0972	.813	2.25
14180	19493	G3IV/V	8.24	76.45	.129				
16107	21313	G0	8.24	71.23	.252				
22429	30339	F8	8.27	73.48	.238	85	3.7961	.913	2.02
24176	33822	G5V	8.19	55.49	.138	115	3.1219	.844	1.98
25436	35996	F3/F5IV	8.23	81.83	.256				
36310	59062	G5	8.20	46.88	.147				
39417	66428	G5	8.33	55.04	.201	86	3.0396	.786	2.27

HIP#	HD#	Type	V	d	[Fe/H]	n	P	χ^2	n_t/n_{ex}
40687	68988	G0	8.27	58.82	.364	145	3.2838	.945	1.01
41777	72579	K0V	8.28	43.18	.136				
43686	76700	G8V	8.23	59.70	.138	109	3.2804	.876	1.35
44823	78277	G2IV	8.25	91.91	.156				
45841	80685	F5/F6V	8.20	77.70	.209	80	3.7714	.777	2.14
53301	94482	G1/G2V	8.18	77.22	.164	123	3.0261	.975	1.36
53424	94690	G5	8.31	52.08	.128				
55076	97854	G0	8.29	81.23	.133				
57468	102361	F8V	8.22	84.46	.318				
60052	107077	F3V	8.29	92.08	.127				
64028	114036	G8III	8.20	52.85	.134				
73408	131664	G3V	8.19	57.21	.156	162	3.5112	.978	1.89
77547	141514	F8V	8.21	66.09	.168				
77641	141599	G6V	8.28	46.38	.181				
81037	148628	F8/G0V	8.22	76.80	.212				
82059	151329	G0	8.23	53.79	.168				
85454	157798	G3V	8.23	92.25	.165				
89247	167081	F8	8.32	49.21	.179				
90593	170469	G5	8.28	64.98	.264				
97769	188015	G5IV	8.29	52.63	.209				
98228	187978	G3V	8.29	84.60	.165				
99034	190613	G3/G5V	8.20	53.48	.193				
111136	213472	G5	8.26	64.35	.126	130	3.7727	.944	1.24
113905	218168	G5	8.18	48.80	.177				
4423	5470	G0	8.42	67.80	.178	63	3.2387	.788	1.85

HIP#	HD#	Type	V	d	[Fe/H]	n	P	χ^2	n_t/n_{ex}
6498	8328	G5	8.36	78.80	.134				
12797	17152	G8V	8.47	44.09	.146	90	3.5859	.880	2.07
15631	21089	G3IV	8.36	68.92	.142	113	3.0146	.871	1.23
16115	22104	G3V	8.40	64.72	.154				
19024	25682	G5	8.39	45.96	.133				
22953	31827	G8IV	8.33	52.49	.274				
27090	38467	G3/G5V	8.33	72.57	.209				
27799	39480	G5	8.42	81.90	.160				
38188	64122	F6/F7V	8.43	73.10	.138				
38636	64273	G5	8.43	55.43	.133	90	3.3756	.910	1.33
45967	80903	G5	8.39	84.89	.139	89	3.0949	.980	2.22
46007	81110	G3V	8.37	46.77	.180				
46325	81505	G8III	8.49	86.81	.237	96	3.3513	.891	2.17
50839	90028	G3V	8.38	83.61	.291				
61880	110314	G2V	8.35	69.54	.187				
65747	117243	G5III	8.41	66.23	.284	121	3.6613	.977	.78
79296	145331	K0/K1III	8.45	65.10	.133				
82757	152776	G5	8.46	86.21	.140	169	3.6598	.879	1.49
106336	204807	G6IV	8.37	64.68	.172				
107397	206683	G3IV	8.39	64.68	.135				
112336	215460	F0	8.42	92.51	.229	78	3.0005	.863	1.26
117526	223498	G7V	8.40	48.66	.140	130	3.3603	.953	2.06
2282	2587	G6V	8.53	48.54	.172				
6197	8038	G5V	8.48	52.97	.200				
7221	9331	G5	8.49	51.07	.251				

HIP#	HD#	Type	V	d	[Fe/H]	n	P	χ^2	n_t/n_{ex}
16727	22282	G5	8.59	50.48	.160				
17269	23398	G5IV/V	8.52	75.19	.214				
21850	30177	G8V	8.49	54.70	.196				
24660	34386	G5III	8.60	53.94	.215				
30377	45133	G5V	8.47	64.81	.156	114	3.9419	.972	2.33
37309	61686	G3V	8.61	72.20	.166				
46871	82606	G0	8.59	67.34	.170	84	3.7138	.920	2.28
48143	85249	F7V	8.58	88.42	.203	137	3.5194	.957	2.39
51877	91702	G5	8.54	52.06	.185				
53624	94861	G0	8.51	90.33	.136				
59968	106937	G6/G8V	8.56	78.43	.149				
60096	107181	G3V	8.49	82.51	.170	96	3.0243	.837	1.16
64955	115762	G2V	8.59	60.35	.129				
70435	126530	G0	8.54	74.91	.169	113	3.7472	.913	2.27
71103	127423	G0V	8.61	69.06	.196	106	3.4208	.906	2.28
80936	149028	G	8.57	48.50	.126				
81269	149396	G5IV/V	8.59	56.24	.127	51	3.5559	.737	2.43
87679	162907	K0V	8.63	48.17	.141				
89321	166745	G5V	8.59	52.03	.143	74	3.9670	.964	1.80
100363	193795	G4IV	8.57	71.33	.245				
104399	201364	A5	8.41	42.25	.470				
105063	202697	G5	8.64	83.13	.168	185	3.2085	.869	1.88
3502	4203	G5	8.75	77.82	.225				
12198	16275	G5	8.72	74.46	.188				
17054	23127	G2V	8.64	89.13	.259	107	3.9807	.850	2.18

HIP#	HD#	Type	V	<i>d</i>	[Fe/H]	<i>n</i>	<i>P</i>	χ^2	n_t/n_{ex}
24110	33811	G8IV/V	8.79	55.99	.250				
43618	75880	G0	8.69	60.64	.125				
49387	87000	G5	8.80	40.50	.143				
51664	91348	G8III	8.73	89.61	.252				
58656	104437	G5IV	8.71	64.72	.182	186	3.5137	.991	1.32
59278	105618	G0	8.71	66.76	.259	106	3.7422	.987	1.81
62350	111069	G5	8.74	59.49	.165				
72041	129401	G8	8.76	92.68	.260	99	3.7066	.894	2.25
81369	149194	F8V	8.72	97.66	.386	114	3.4416	.989	1.18
104182	201093	G5	8.69	96.90	.175				
109355	210312	G5	8.71	55.90	.179				
116517	221954	G5/G6V	8.82	98.81	.211	96	3.1993	.940	1.50
116984	222697	G5	8.73	43.76	.143				
5807	7487	F7V	8.86	94.43	.168				
5881	7483	G5	8.94	59.17	.254	94	3.7366	.909	2.04
19126	26071	G5IV/V	8.97	91.16	.130	137	3.9492	.964	1.70
21889	30295	K0/K1V	8.94	58.34	.150				
23069	31609	G5	8.99	50.86	.158	90	3.0239	.924	1.85
54104	96020	G8V	8.89	77.34	.278				
54381	96529	G5	8.93	77.10	.158				
61028	108874	G5	8.84	68.54	.138	96	3.2223	.992	2.11
65882	117497	G0III	8.80	78.62	.167				
66621	118914	G0	8.90	73.75	.304	143	3.1064	.961	1.78
69660	124595	G1/G2V	8.85	76.86	.148	68	3.1879	.683	2.12
72203	129445	G6V	8.85	67.61	.246				

HIP#	HD#	Type	V	d	[Fe/H]	n	P	χ^2	n_t/n_{ex}
109207	209913	G8V	8.86	69.64	.158				
109428	210392	G0	8.80	90.50	.280				
116756	222342	F0	8.90	79.05	.191				
117427	223315	G5V	8.87	53.62	.203				
4752	5946	G5	9.01	91.24	.154	78	3.2105	.875	1.85
5389	6880	G8/K0V	9.20	46.36	.248				
20273	27496	G5	9.03	92.51	.133				
21703	29528	K0	8.99	56.69	.206				
27688	39503	G5IV/V	9.04	63.53	.138				
29550	43197	G8/K0IV	9.03	54.95	.180	123	3.6620	.995	2.05
42084	72680	K0	9.00	51.63	.200	64	3.0322	.737	2.37
44279	77417	G8IV	9.10	65.06	.192				
45982	80606	G5	9.01	58.38	.195				
46113	81270	F6V	9.01	91.83	.253	88	3.2640	.925	2.36
62198	110855	G0	9.11	80.65	.138	101	3.3616	.883	1.77
101982	340795	G5	8.99	75.82	.182				
114967	219556	K0V	9.19	58.17	.136				
9550	12585	G3V	9.29	77.40	.233				
22320	30669	G8/K0V	9.17	54.91	.142	151	3.8691	.955	1.52
46639	233641	G0	9.28	96.62	.335				
57735	102843	K0	9.32	54.44	.172				
58318	103829	F8	9.29	89.21	.274				
61123	108953	G8/K0IV/	9.36	63.73	.176				
62093	110605	G8V	9.21	71.68	.162				
78521	143361	G6V	9.24	59.35	.204	96	3.2201	.789	1.81

HIP#	HD#	Type	V	d	[Fe/H]	n	P	χ^2	n_t/n_{ex}
82632	152079	G6V	9.27	85.18	.186	85	3.4298	.804	1.78
88631	165204	G6/G8V	9.20	75.87	.165				
97125	186265	G8V	9.29	86.81	.138	86	3.1557	.880	2.00
117882	224040	F3/F5V	9.27	84.18	.354				
5311	6790	G0V	9.43	87.80	.363				
27113	38554	G6V	9.46	82.78	.140				
48809	86397	G8V	9.62	69.40	.179				
94552	179640	G6V	9.56	91.16	.201				
94615	230999	G5	9.76	99.30	.410				
104226	200869	K1IV/V	9.48	63.65	.206				
33634	52217	G8V	9.98	74.35	.156				